Supporting Information

Near-infrared Emission, Energy Transfer, and Mechanisms of Mn^{2+} and Cr^{3+} Co-doped Lead-free $Cs_2AgInCl_6$ Double Perovskites

Daiwen Chen[a], Huayuan Li[a], Cu Wu[a], Liya Zhou[a], Peican Chen[a], Qi Pang[a], Xinguo Zhang[b] and Jin Zhong Zhang[c]*

[a] Guangxi Key Laboratory of Petrochemical Resource Processing and Process Intensification Technology, School of Chemistry and Chemical Engineering, Guangxi University, Nanning 530004, Guangxi, Peoples R China

[b] School of Pharmaceutical Sciences, Southern Medical University, Guangzhou 510515, Peoples R China

[c] Department of Chemistry and Biochemistry, University of California, Santa Cruz, California 95064, United States

Corresponding authors: pqigx@163.com

Experimental

1. Chemicals

CsCl (99%, Aladdin), $InCl_3$ (99.99%, Aladdin), AgCl (99.5, Macklin), $CrCl_3 \cdot 6H_2O$ (analytical pure, Aladdin), $MnCl_2$ (99.99%, Aladdin), hydrochloric acid (HCl, analytical pure, Chengdu Kelong Chemical Reagent Factory, China) were all purchased and used as received without further purification.

2. Synthesis of CAIC: xMn^{2+} DPSCs (x=0.0100, 0.0300, 0.0500, 0.0700, 0.0900 and 0.110 mmol)

Mn^{2+} doped $Cs_2AgInCl_6$ DPSCs were prepared following a hydrothermal method. Solid CsCl (0.337 g, 2.00 mmol), $InCl_3$ (0.221 g, 1.00 mmol), AgCl (0.1433 g, 1.00 mmol) and $MnCl_2$ (x=0.0100, 0.0300, 0.0500, 0.0700, 0.0900, 0.1100mmol) were mixed with 15.0 ml (10.0 M) HCl in a 50 cm^3 Teflon autoclave. Varied Mn^{2+} doping concentrations are achieved by changing the Mn^{2+} amounts during the synthesis. The solution was heated at 150 °C for 12 h, then slowly and steadily cooled to 60 °C at a speed of 3 °C per hour in a Teflon-lined stainless steel autoclave and maintained at a constant temperature of 60 °C. The as-prepared crystals were filtered out and washed with isopropanol and dried in a furnace at 60°C for 3 hours. The corresponding samples are noted as CAIC: xMn^{2+} DPSCs (x=0.0100, 0.0300, 0.0500, 0.0700, 0.0900 and 0.1100)

3. Synthesis of CAIC: 0.09Mn^{2+}, yCr^{3+} (y=0.0100, 0.0500, 0.100, 0.200, 0.300 and 0.400 mmol)

The synthesis method used is similar to the CAIC: xMn^{2+} DPSCs except for additionally adding different amount of $CrCl_3 \cdot 6H_2O$ with 0.0100, 0.0500, 0.100, 0.200, 0.300 and 0.400 mmol. The corresponding samples are noted as CAIC: 0.09Mn^{2+}, yCr^{3+} (y=0.0100, 0.0500, 0.100, 0.200, 0.300 and 0.400 mmol).

4. Characterization

The powders used were all obtained by grinding in a mortar. SMARTLAB3KW powder diffractometer measured the X-ray diffraction (XRD) patterns with the Cu Kα radiation source at a voltage of 40 kV and 30 mA. The morphology and size of the DPSCs were characterized by Scanning Electron Microscope (SEM). The elemental

composition and distribution of the materials were observed by energy-dispersive X-ray spectroscopy (EDS) coupled with SEM. Inductively coupled plasma optical emission spectroscopy (ICP-OES) was performed on an Agilent 720ES instrument. X-ray photoelectron spectroscopy (XPS) was measured with Thermo Fisher Scientific Company in the United States of Escalab250Xi X-ray photoelectron spectrometer. Electron paramagnetic resonance (EPR) spectra were measured by a Bruker-A300-10/12 spectrometer. Measurements were done at room temperature with a 9.86 GHz microwave frequency, 4 G modulation amplitude and a power of 2 mW. UV-vis diffuse reflectance spectra were measured using the Techcomp UV2600 UV-vis spectrophotometer. PL, PLE, TRPL, and Temperature-dependent PL were measured by FLS1000 fluorescence spectrometer of Edinburgh instruments utilizing the xenon lamp (Xe900) for excitation. (The detectors used for measuring the PL include a visible range signal detector with spectral coverage from 230 nm to 800 nm and a NIR signal detector with spectral coverage from 800 nm to 1700 nm) PLQY was measured by integrating sphere and Hamamatsu quantum yield measurement system.

5. Screen printing

We mixed the CAIC: Mn^{2+}, Cr^{3+} DPSCs powder with terpilenol. Pouring the mixed slurry onto one end of the printed template with the patterns, and the blade was used to apply appropriate pressure to the ink slurry on the printing screen plate, while moving evenly toward the other end. The expected uniform patterns form during the movement. Then, the substrate was heated to 60 °C to remove the solvent.

6. Calculation of bandgap

The optical bandgap of the phosphor can be calculated using the Kubelka–Munk model to convert the absorption spectrum of the phosphor into function[1].

$$F(R) = \frac{(1-R)^2}{2R} \tag{1}$$

$$\alpha h\nu = c(h\nu - E_g)^{\frac{1}{2}} \tag{2}$$

$$[(h\nu F(R_\infty))]^2 = A(h\nu - E_g) \tag{3}$$

where R is the diffuse reflection of the spectrum, α is the linear absorption coefficient, hν is the energy of light, c is a constant, A is a constant, E_g is the direct bandgap, and R∞ represents the reflectance of the infinitely thick sample with respect to a reference at each wavelength. On making a tangent at the inflection point of the curve, the hν value at the intersection of the tangent and the horizontal axis is the bandgap (E_g) value.

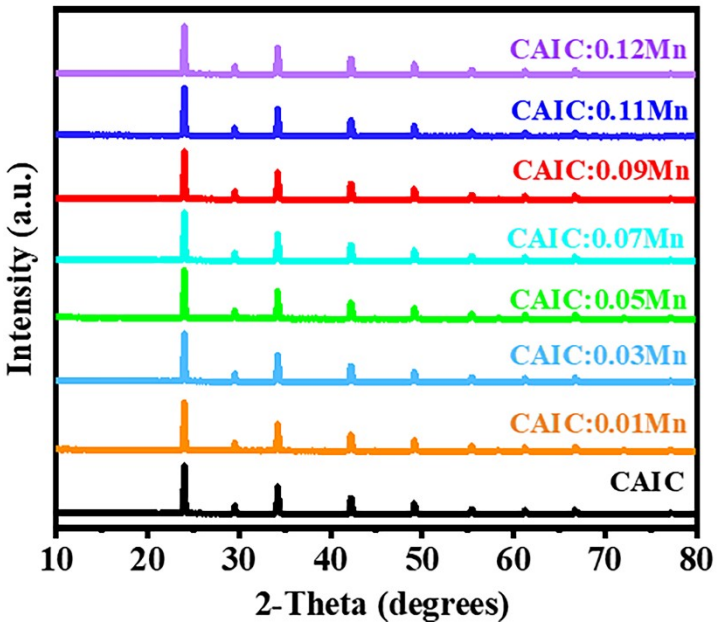

Figure S1. XRD patterns of Mn^{2+} doped CAIC DPSCs.

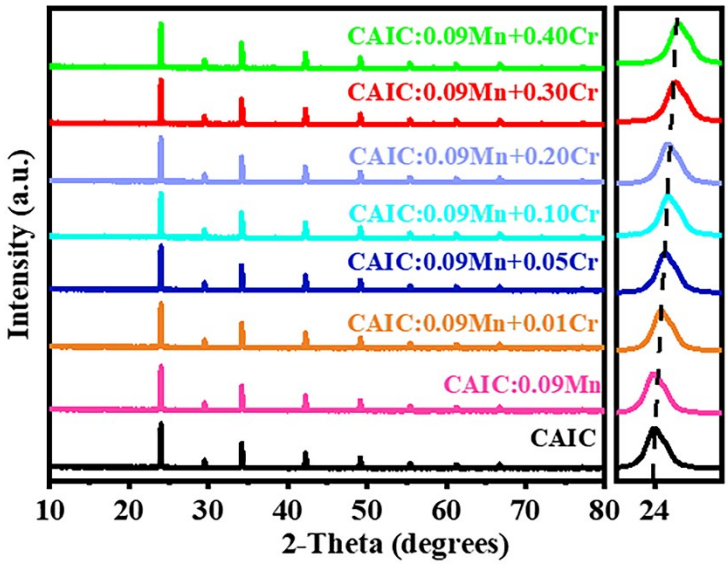

Figure S2. XRD patterns of CAIC: 0.05Mn^{2+}, yCr^{3+}(x = 0-0.400) DPSCs and (220) local enlarged view of crystal plane.

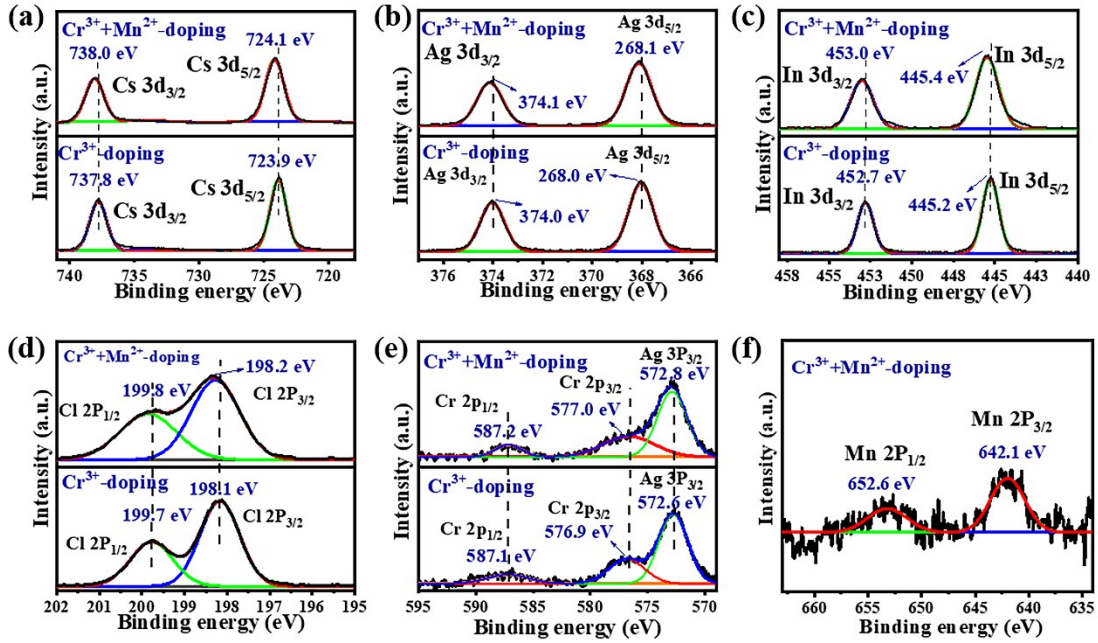

Figure S3. X-ray photoelectron spectroscopy (XPS) core level spectra of (a) Cs 3d, (b) Ag 3d, (c) In 3d, (d) Cl 2p, (e) Cr 2p, (f)Mn 2p.

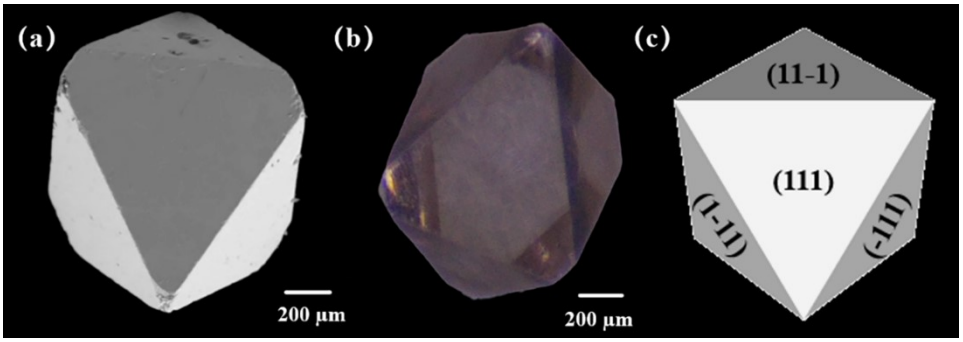

Figure S4. (a) The SEM images of CAIC: Mn^{2+}, Cr^{3+} DPSCs. (b) photographs of DPSCs obtained via an optical microscope (c) and the simulated crystal faces for one crystal particle.

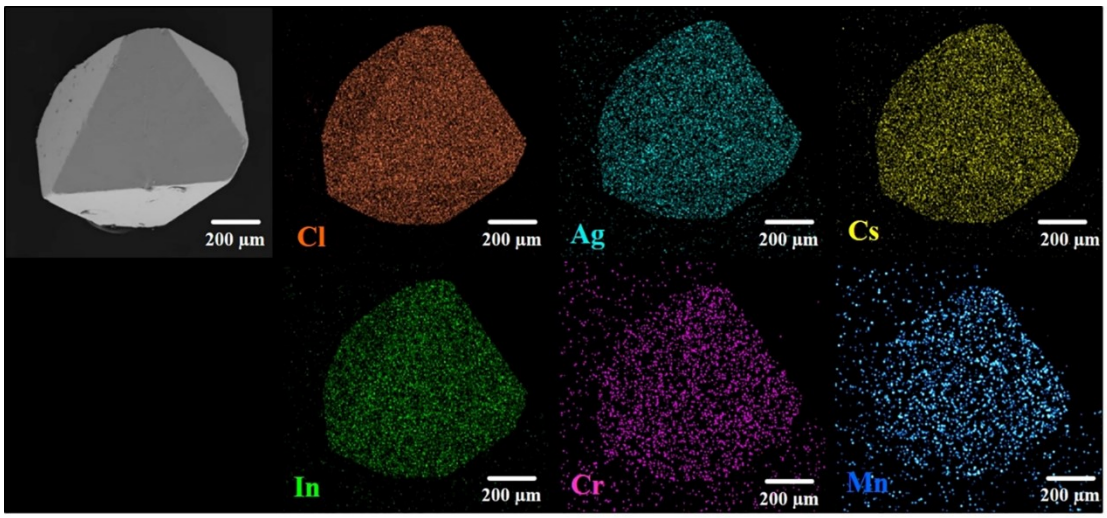

Figure S5. SEM image and EDS spectra of CAIC: Mn^{2+}, Cr^{3+} DPSCs with the corresponding atomic maps.

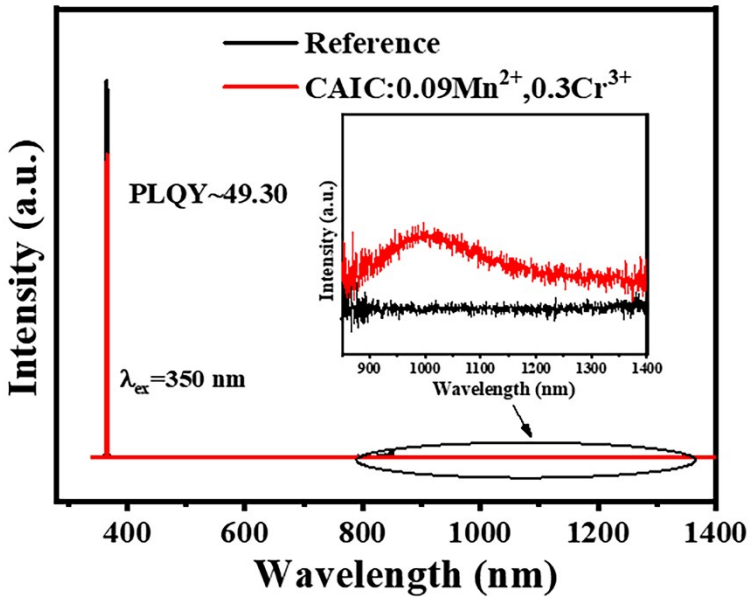

Figure S6. Luminescent spectra for the PLQY measurement of CAIC: $0.09Mn^{2+}$, $0.3Cr^{3+}$.

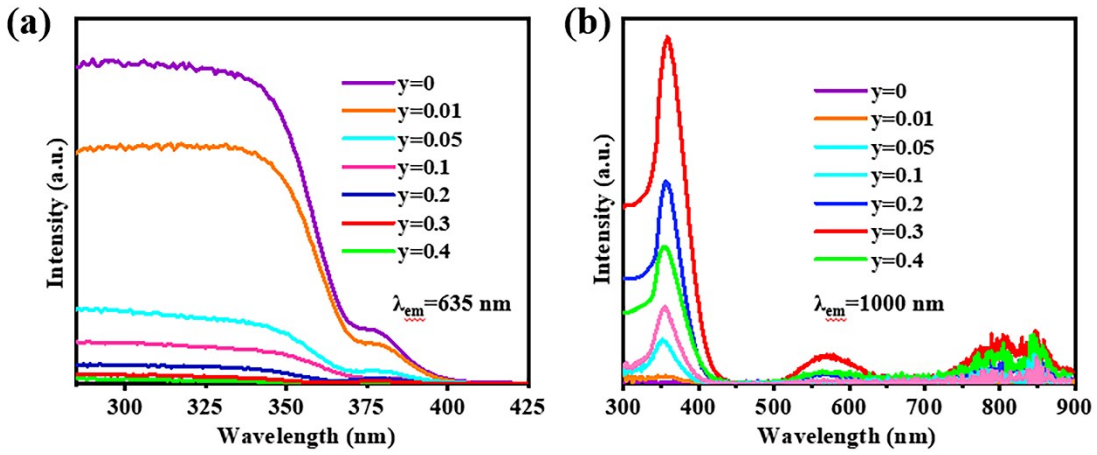

Figure S7. (a and b) PLE spectra of CAIC: $0.09Mn^{2+}$, yCr^{3+} with emission at (a) 635 nm and (b) 1000 nm.

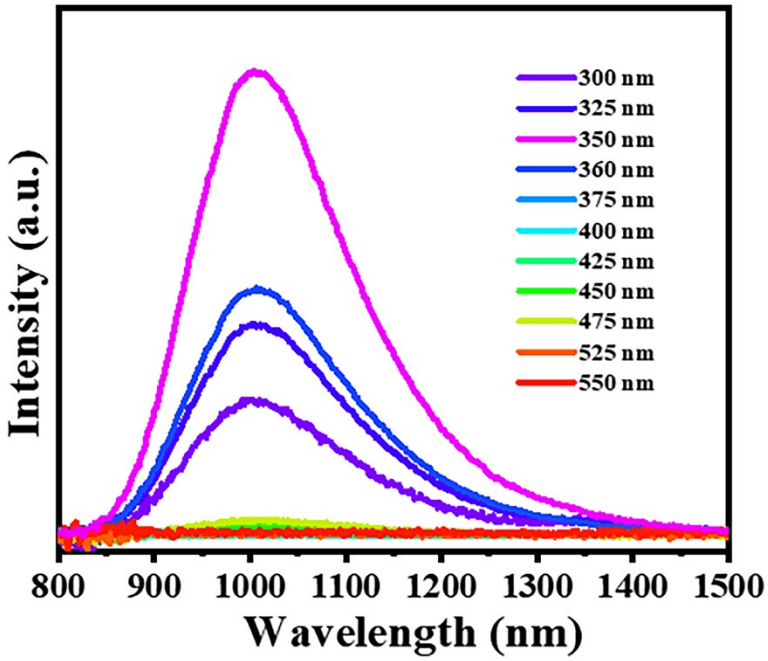

Figure S8. Excitation-wavelength-dependent (300-550 nm) PL spectra of CAIC: 0.09 Mn^{2+}, 0.30Cr^{3+}.

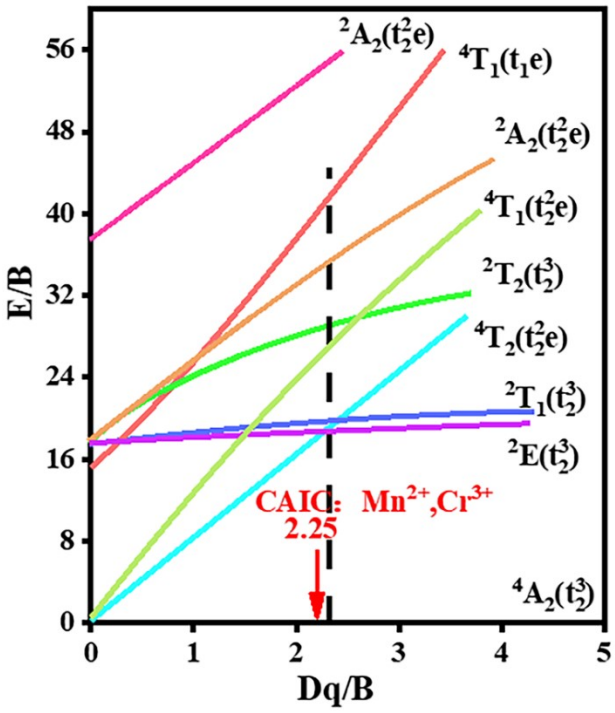

Figure S9. Tanabe-Sugano energy level diagram of Cr^{3+} in an octahedral crystal field.

According to energy level splitting, the weak crystal field and the strong crystal field are defined by the intersection of $^4T^2$ and ^2E energy levels[2]. The following

equations can be used to obtain D_q/B:

$$D_q = E(^4A_2 \rightarrow {}^4T_2)/10 \quad (4)$$

$$\frac{Dq}{B} = \frac{15\left(\frac{\Delta E}{Dq} - 8\right)}{(\Delta E/Dq)^2 - 10(\Delta E/Dq)} \quad (5)$$

In the above equations, D_q and B are the crystal field splitting energy and Racah parameter, respectively, and ΔE is the energy difference between E ($^4A_2 \rightarrow {}^4T_1$) and E ($^4A_2 \rightarrow {}^4T_2$) transitions, obtained by the peak of the absorption band. Based on eqn (4) and (5), the calculated values of D_q and B are about ~1204 and 533 cm^{-1} respectively. The results in a D_q/B value of 2.25 (Figure S9), which is less than 2.30, and thus Cr^{3+} will generate broadband NIR emission in this host.

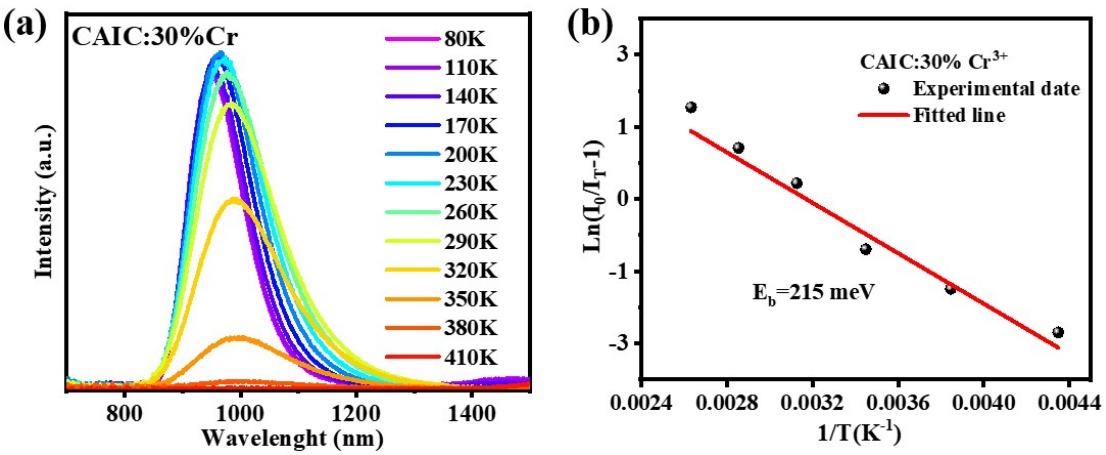

Figure S10. (a) Temperature-dependent PL spectra of CAIC: 0.30Cr^{3+} DPSCs under 350 nm excitation. (b) Ln(I_0/I_T–1) versus 1/T plot of the temperature dependent spectra.

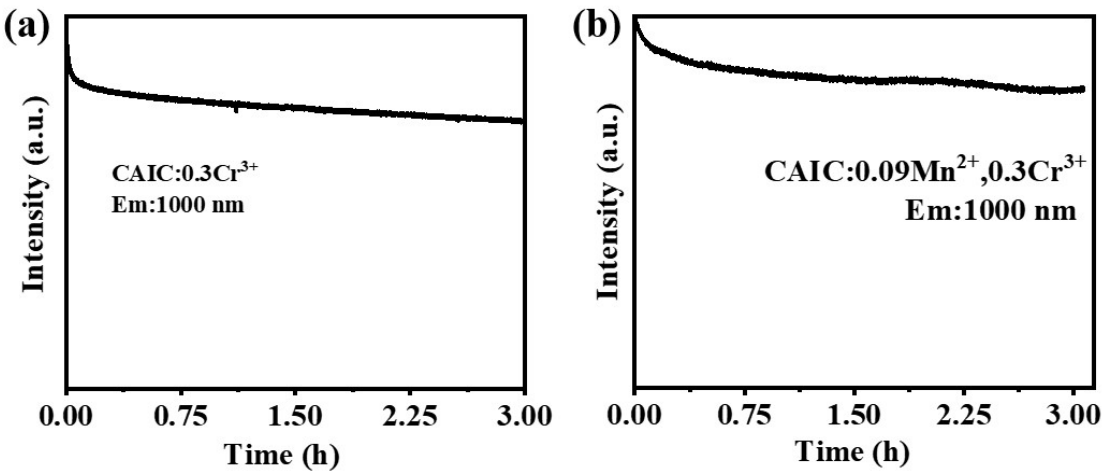

Figure S11. The PL intensity of CAIC:0.3Cr^{3+} and CAIC: 0.09Mn^{2+}, 0.3Cr^{3+} exposed at 350 nm UV light for 3h.It shows the PL intensity dependence of irradiation time.

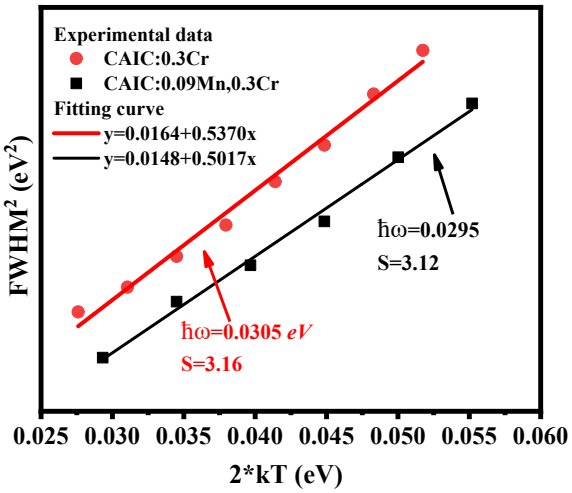

Figure S12. The fitting results of $FWHM^2$ as a function of 2kT.

Table S1 Mn^{2+} and Cr^{3+} content from starting materials and measured by ICP.

CAIC: $0.09Mn^{2+}$, yCr^{3+}			
Cr^{3+}		Mn^{2+}	
Nominal (atomic ratio %)	ICP-OES (atomic ratio %)	Nominal (atomic ratio %)	ICP-OES (atomic ratio %)
0	0	9	0.0270
1	0.0030	9	0.0202
5	0.0063	9	0.0200
10	0.0151	9	0.0201
20	0.0325	9	0.0201
30	0.0417	9	0.0202

Table S2 The detailed analysis of decay curves for CAIC: $0.09Mn^{2+}$, yCr^{3+}.

CAIC: $0.09Mn^{2+}$, yCr^{3+}, monitored at 635nm					
Sample	$\mathbf{A_1}$	$\mathbf{A_2}$	τ_1	τ_2	τ_{ave}
0.09Mn	15465.25	3773.54	114.23	578.58	370.8986
0.01Cr	41148.89	2778.12	72.74	326.13	131.6184
0.05Cr	91348.75	2115.46	63.6	351.4	96.24728
0.1Cr	146825.7	1575.37	41.79	359.88	68.6951
0.2Cr	274442.4	1373.26	43.5	394.87	58.7665
0.3Cr	272260.64	981.295	33.49	360.6	45.71035
0.4Cr	352230.5	601.96	33.93	145.42	34.74068

Table S3 The detailed analysis of decay curves for CAIC: $0.09Mn^{2+}$, yCr^{3+}.

CAIC: $0.09Mn^{2+}$, yCr^{3+}, monitored at 1000 nm					
Sample/y	0.0100	0.0500	0.100	0.200	0.300
τ/μs	9.20	11.2	15.2	17.1	19.8

References

1. A. K. Bedyal, V. Kumar, R. Prakash, O. M. Ntwaeaborwa and H. C. Swart, *Applied Surface Science*, 2015, **329**, 40-46.

2. A. Lever, *The Crystal Field Splitting Parameter Dq: Calculation and Significance*, Werner Centennial, **1967**.